

Demonstrating a gyrator operation using Josephson mixers

Baleegh Abdo, Markus Brink, and Jerry M. Chow

IBM T. J. Watson Research Center, Yorktown Heights, New York 10598, USA.

(Dated: February 7, 2017)

Nonreciprocal microwave devices such as circulators are useful in routing quantum signals in quantum networks and protecting quantum systems against noise coming from the detection chain. However, commercial, cryogenic circulators, used nowadays, are unsuitable for scalable superconducting quantum architectures due to their appreciable size, loss, and inherent magnetic field. In this work, we report on the measurement of a key nonreciprocal element, i.e., the gyrator, which can be used to realize a circulator. Unlike state-of-the-art gyrators, which use a magneto-optic effect to induce a phase shift of π between transmitted signals in opposite directions, our device uses the phase nonreciprocity of a Josephson-based three-wave mixing device. By coupling two of these mixers and operating them in noiseless frequency conversion mode, we show that the device acts as a nonreciprocal phase shifter, whose phase shift is controlled by the phase difference of the microwave tones driving the mixers. Such a device could be used to realize a lossless, on-chip, superconducting circulator suitable for quantum information processing applications.

Performing high-fidelity, quantum nondemolition measurements in the microwave domain is an important requirement for operating a superconducting quantum computer. Such a requirement is enabled, in various schemes, by using nonreciprocal microwave devices having asymmetrical transmission through their ports, such as circulators [1–8] and low-noise, directional amplifiers [3, 9–11, 13]. In particular, circulators play several crucial roles in these measurement schemes. They 1) allow quantum systems to be measured in reflection, 2) enable the use of reflective Josephson parametric amplifiers (JPAs) as a first-stage amplifier in the output chain, 3) protect quantum systems against noise in the measurement chain, such as amplified signals reflected off JPAs, excess back-action of directional amplifiers, strong microwave tones feeding JPAs, and noise coming from higher amplification stages of the output line. However, state-of-the-art, commercial, cryogenic circulators, ubiquitously used throughout the field today, limit the maximum achievable measurement fidelity and scalability of quantum processors, due to their insertion loss ~ 0.5 dB, large size ~ 28 cm³, and weight ~ 41 g [14]. They can also potentially negatively affect the coherence times of qubits, as they are comprised of bulk materials that thermalize poorly and employ strong inherent magnetic fields 10 – 100 G [14].

In this work, we demonstrate a successful operation of an important nonreciprocal circuit element, i.e., a gyrator, which can be used to build a circulator. A gyrator is a two-port, unity-transmission device, which introduces a differential phase shift of 180° to microwave signals transversing the device in opposite directions [1]. By incorporating an on-chip, lossless gyrator into one arm of a Mach-Zender interferometer, employing two hybrids [1], it is straightforward to realize a four-port, on-chip, lossless circulator suitable for scalable quantum processors. In contrast to standard gyrator realizations, which utilize a magneto-optic Faraday effect in order to induce a nonreciprocal phase shift between microwave beams propagating in opposite directions, our scheme is based

on different physics. It utilizes a dispersive, three-wave mixing process, in which the phase of the pump drive imprints a nonreciprocal phase shift on the propagating waves through the device. As a result of this fundamental difference in the device physics, the main advantage of our proposed gyrator scheme over standard realizations is that it neither employs magnetic materials nor strong permanent magnets for its operation. Therefore, it can be low loss, integrated on chip, and fully compatible with superconducting circuits for extensible architectures.

While there have been numerous promising schemes which have been shown recently, either experimentally or theoretically, to perform a circulation operation suitable for quantum signals [2–8], the main two differences between our proposed scheme and those relying on frequency conversion between three modes of a Josephson-based superconducting device, namely Refs. [3] and [6], are that our proposed circulator scheme preserves the frequency of the input and output quantum signals, and requires, in principle, only one pump tone instead of three. This can result in a significant reduction in the overall control hardware resource for operating a larger number of devices.

The nonreciprocal phase shifter scheme, used to demonstrate a gyrator operation, employs two dissipationless, nondegenerate three-wave mixers. The general scheme for the two-port, nonreciprocal phase shifter is depicted in Fig. 1 (a). It consists of two unitary frequency conversion stages (i.e., three-wave mixers) connected together by a transmission line. Incoming signals at frequency f_1 on port 1 (2) of the device are upconverted using the first (second) frequency conversion stage to frequency f_2 ($f_2 > f_1$) and transmitted via the transmission line to the second (first) frequency conversion stage, where it is downconverted back to f_1 and exits through port 2 (1). Both frequency conversion processes taking place in the device, i.e., upconversion and downconversion, are enabled via energy exchange with the pump drives feeding the two mixing stages at a certain power, and whose frequency f_p corresponds to the frequency dif-

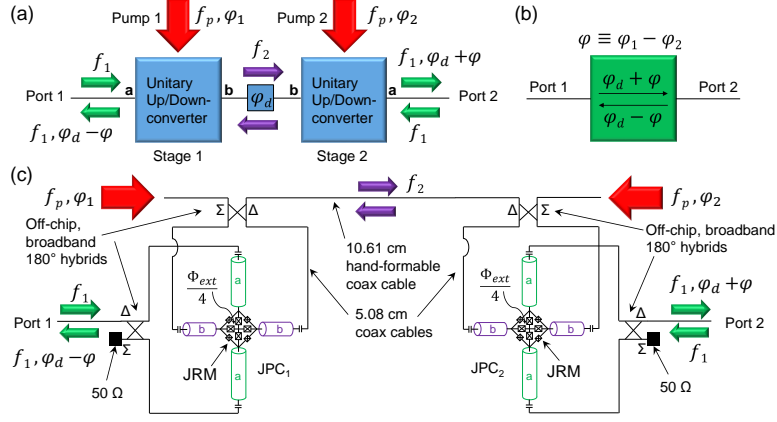


FIG. 1: (color online). (a) A nonreciprocal phase shifter scheme, which comprises of two coupled, nondegenerate three-wave mixing devices capable of performing unitary frequency conversion. Each three-wave mixing device has two ports a and b , which support incoming and outgoing signals at frequency f_1 and f_2 respectively (where $f_2 > f_1$). In the exemplary scheme shown in panel (a), the two devices are coupled through port b . The device transmits with frequency conversion input signals at f_1 (f_2) on port a (b) to output signals on port b (a) at f_2 (f_1). The frequency conversion process is enabled through energy exchange with the pump drive, feeding the three-wave mixing device at frequency $f_p = f_2 - f_1$. The nonreciprocal phase shift imprinted on the transmitted signals through the device (from port 1 to 2 and vice versa) is set by the phase difference between the two pump drives feeding the two three-wave mixing stages φ and the electrical delay between them (i.e., the phase shift φ_d). (b) A black-box representation of the nonreciprocal phase shifter. Signals transmitted through the device acquire a phase shift of $\varphi_d + \varphi$ from port 1 to 2 versus $\varphi_d - \varphi$ in the opposite direction. (c) A proof-of-principle nonreciprocal phase shifter device realized by coupling the idler ports of two nominally identical JPCs, operating in frequency conversion mode, via a 10.61 cm normal-metal coax cable. The fabrication process of the JPCs is the same as in Ref. [15].

ference $f_p = f_2 - f_1$. In addition to the critical role played by the pump power and frequency in the operation of the device, which will be made clear below, the pump phase plays a pivotal role as well. It controls the nonreciprocal phase shift experienced by the transmitted signals from port 1 to 2, i.e., $\varphi_d + \varphi$, versus the phase shift $\varphi_d - \varphi$ acquired in the opposite direction, where $\varphi \equiv \varphi_1 - \varphi_2$ is the phase difference between the two pump drives feeding the two mixing stages and φ_d is the phase shift introduced by the connecting components. In Fig. 1 (b), we exhibit a black-box representation of the device, which emphasizes the nonreciprocal phase shift introduced by the device and its dependence on the phase difference between the two pump drives feeding the system. In Fig. 1 (c), we show in more detail how the proof-of-principle device is realized, i.e., by using two separate, nominally identical, Josephson parametric converters (JPCs) [16], connected through a 10.61 cm coax line.

In general, JPCs are used as quantum-limited JPAs for qubit readout [17, 18], but they can also function as dissipationless, three-wave mixers [19, 20]. As seen in Fig. 1 (c), the JPC comprises a Josephson ring modulator (JRM) embedded at the center of two orthogonal, half-wavelength microstrip resonators denoted a and b . The JRM consists of four Josephson junctions (JJs) arranged in a Wheatstone bridge configuration and functions as a nonlinear, dispersive mixing element. The resonators a and b support two microwave tones denoted signal (S) (at frequency f_1) and idler (I) (at frequency f_2) respec-

tively. These tones lie within the bandwidths $\gamma_a/2\pi$ and $\gamma_b/2\pi$ of resonators a and b , whose fundamental modes, at frequencies $\omega_a/2\pi$ and $\omega_b/2\pi$, have an rf-current anti-node at the JRM location. Both resonators are capacitively coupled to external feedlines that carry microwave signals into and out of the JPC. To address the a and b modes and apply the pump drive (P) to the device, both S and I tones are fed through the delta ports of two off-chip, broadband 180° hybrids, while the pump at $f_p = \omega_p/2\pi$ is fed through the sigma port of the hybrid connected to port b (the other sigma port connected to port a is terminated by a 50 Ohm cold load). Furthermore, to facilitate the mixing operation in the device, a dc circulating current is induced in the outer loop by an external magnetic flux threading the JRM [16]. The four large JJs inside the JRM loop serve as a linear shunt inductance for the outer JJs, which lifts the hysteretic response of the JRM versus flux and therefore makes the resonance frequencies of the JPC tunable [21].

Figure 2 (a) shows a signal flow graph for a JPC operated in frequency conversion mode. In the stiff pump approximation, the scattering parameters of the device read [16]

$$\begin{aligned} r_{aa} &= \frac{\chi_a^{-1*} \chi_b^{-1} - |\rho|^2}{\chi_a^{-1} \chi_b^{-1} + |\rho|^2}, & t_{ab} &= \frac{2i|\rho|e^{-i\varphi_p}}{\chi_a^{-1} \chi_b^{-1} + |\rho|^2}, \\ r_{bb} &= \frac{\chi_a^{-1} \chi_b^{-1*} - |\rho|^2}{\chi_a^{-1} \chi_b^{-1} + |\rho|^2}, & t_{ba} &= \frac{2i|\rho|e^{i\varphi_p}}{\chi_a^{-1} \chi_b^{-1} + |\rho|^2}, \end{aligned} \quad (1)$$

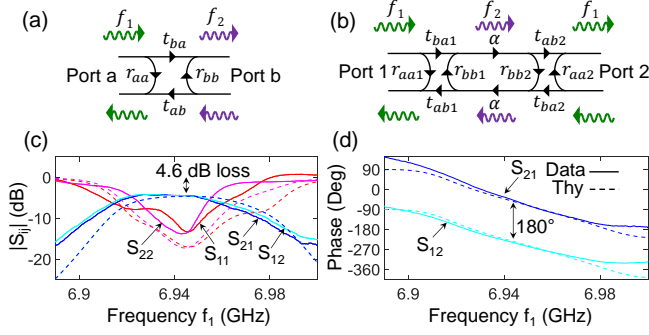


FIG. 2: (color online). (a) Signal flow graph for a JPC device operating in frequency conversion mode. (b) Signal flow graph for a two-stage JPC (TSJPC) device. The two JPCs are coupled through their idler ports using a lossy transmission line. (c) Magnitude measurement (solid) and calculation (dashed) of the scattering parameters of the TSJPC device operated in frequency conversion mode versus input frequency f_1 . (d) Phase measurement (solid) and calculation (dashed) of the transmission parameters of the TSJPC device versus input frequency f_1 . The phase measurement exhibits a differential phase of 180° on resonance, which is a distinct feature of a gyrator. The device parameters used in the calculation are: $\omega_p/2\pi = 3.332$ GHz, $\omega_{a1}/2\pi = 6.948$ GHz, $\gamma_{a1}/2\pi = 60$ MHz, $\gamma_{b1}/2\pi = 55$ MHz, $\omega_{a2}/2\pi = 6.945$ GHz, $\gamma_{a2}/2\pi = 50$ MHz, $\gamma_{b2}/2\pi = 45$ MHz, $\tau_d = 0.847$ ns, $|\rho| = 0.9$, $|\alpha| = 0.596$, $\varphi_1 = \pi/2$, $\varphi_2 = 0$.

where r_{aa} (r_{bb}) is the reflection parameter off port a (b), t_{ba} (t_{ab}) is the transmission parameter from port a (b) to port b (a) with frequency upconversion (downconversion), and $|\rho|$ is a dimensionless pump amplitude. In Eq. (1) the χ 's are the bare response functions of modes a and b (whose inverses depend linearly on the S and I frequencies):

$$\begin{aligned} \chi_a^{-1}[\omega_1] &= 1 - 2i \frac{\omega_1 - \omega_a}{\gamma_a}, \\ \chi_b^{-1}[\omega_2] &= 1 - 2i \frac{\omega_2 - \omega_b}{\gamma_b}. \end{aligned} \quad (2)$$

Since the applied pump frequency satisfies the relations $\omega_p = \omega_b - \omega_a = \omega_2 - \omega_1$, χ_b^{-1} of Eq. 2 can be rewritten as $\chi_b^{-1}[\omega_1] = 1 - 2i(\omega_1 - \omega_a)/\gamma_b$. The scattering parameters of Eq. 1 embody five important properties that are crucial for understanding the device physics: 1) the scattering matrix is unitary (the total number of photons is conserved), i.e., the following relations hold $|r_{aa}|^2 + |t_{ab}|^2 = 1$ and $|r_{bb}|^2 + |t_{ba}|^2 = 1$; 2) the transmitted signals from port a to b (b to a) undergo frequency upconversion (downconversion); 3) on resonance ($\omega_{1,2} = \omega_{a,b}$) and for a sufficiently large pump drive $|\rho| \rightarrow 1^-$, the reflections off the device ports vanish ($|r| \rightarrow 0$), while the transmission with frequency conversion approaches unity ($|t| \rightarrow 1$); 4) the phase of the transmitted signals depends on the phase of the pump drive φ_p (as seen in the expressions

for t_{ab} and t_{ba} in Eq. 1); 5) the phase shift acquired by signals transverting the device is nonreciprocal (i.e., φ_p from port a to b and $-\varphi_p$ in the opposite direction).

The signal flow graph for the two-stage JPC (TSJPC) device is shown in Fig. 2 (b). The scattering parameters in the graph with the subscript 1 (2) correspond to those of JPC 1 (2). The parameter $\alpha = |\alpha|e^{i\varphi_d}$ incorporates the amplitude attenuation coefficient $|\alpha|$ and the phase shift $\varphi_d = \omega_2\tau_d$ experienced by the idler signals propagating between the two JPC stages at frequency f_2 . In the expression for φ_d , τ_d represents the delay time, which can in turn be expressed as $\tau_d = l_d\sqrt{\epsilon}/c$, where c is speed of light, l_d and ϵ are the effective electrical length and dielectric constant of the coax-lines and hybrids connecting the two stages, respectively. By inspection, the scattering parameters of the two-port device can be written in the form [1]

$$\begin{aligned} S_{11} &= r_{aa1} + \frac{r_{bb2}t_{ba1}t_{ab1}\alpha^2}{1 - r_{bb1}r_{bb2}\alpha^2}, & S_{12} &= \frac{t_{ab1}t_{ba2}\alpha}{1 - r_{bb1}r_{bb2}\alpha^2}, \\ S_{22} &= r_{aa2} + \frac{r_{bb1}t_{ba2}t_{ab2}\alpha^2}{1 - r_{bb1}r_{bb2}\alpha^2}, & S_{21} &= \frac{t_{ab2}t_{ba1}\alpha}{1 - r_{bb1}r_{bb2}\alpha^2}, \end{aligned} \quad (3)$$

where S_{11} (S_{22}) is the reflection parameter off port 1 (2), S_{21} (S_{12}) is the transmission parameter from port 1 to 2 (2 to 1) (with frequency preservation). Similar to the case of one JPC, on resonance ($\omega_{1,2} = \omega_{a,b}$) and for a sufficiently large pump drive $|\rho| \rightarrow 1^-$, the reflections off the device ports vanish ($S_{11}, S_{22} \rightarrow 0$), while the transmission amplitude approaches the attenuation amplitude set by the losses in the connecting stages ($|S_{12}|, |S_{21}| \rightarrow |\alpha|$). However, the phase acquired by the transmitted signals on resonance from port 1 to 2, i.e., $\angle S_{21} = \varphi_d + \varphi$ can be different from the phase acquired in the opposite direction, i.e., $\angle S_{12} = \varphi_d - \varphi$. While the total phase shift in each direction depends on the value of φ_d and φ , the differential phase between the two directions depends only on φ , i.e., $\angle S_{21} - \angle S_{12} = 2\varphi$. Thus, by setting the pump phase difference to $\pi/2$, the TSJPC device can serve as a gyrator, which introduces a differential phase of π between signal beams propagating in opposite directions.

In Fig. 2 (c) and (d), we demonstrate a gyrator operation using the TSJPC device. In Fig. 2 (c), we depict using solid lines a network analyzer magnitude measurement of the scattering parameters of the TSJPC device taken versus input frequency f_1 . The resonance frequencies of resonators a of the two stages are flux-tuned to coincide at 6.945 GHz and both JPCs are operated in frequency conversion mode with $f_p = 3.332$ GHz. The measurement of the four scattering parameters of the device is enabled by connecting each port of the device to separate input and output lines via a three-port cryogenic circulator. As expected, at resonance, the reflection parameters S_{11} (red), S_{22} (magenta) exhibit a dip $\simeq -15$ dB, while the transmission parameters S_{21} (blue), S_{12} (cyan) exhibit a peak of about $\simeq -4.6$ dB, which matches the insertion loss of the microwave components connect-

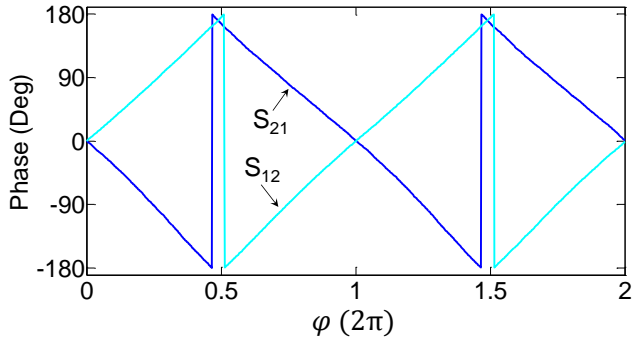


FIG. 3: (color online). A network analyzer phase measurement of the transmission parameters (i.e., S_{21} and S_{12}) of the TSJPC device taken on resonance for varying phase difference between the applied pump drives feeding the two stages. The device working point is the same as in Fig. 2 (c). A constant phase offset is applied to both curves in order to center them around zero phase.

ing the two stages at frequency f_2 , i.e., the normal-metal coax cables and hybrids. In Fig. 2 (d), we exhibit a phase shift measurement of the transmitted signals S_{21} (solid blue) and S_{12} (solid cyan), versus input frequency f_1 . The phase measurement is taken at the same working point as Fig. 2 (c). The phase difference between the pump drives feeding the two JPC stages is set to yield a relative phase shift of about 180° between signals transmitted in opposite directions. Dashed lines in Figs. 2 (c), (d) exhibit a theoretical calculation for the scattering parameters of the device based on Eq. 3 and the device parameters, which yields a relatively good agreement with the data. It is interesting that the calculation reproduces multiple unintuitive features seen in the experiment (Fig. 2 (c)), such as bends and plateaus, which can be attributed to dispersion effects of the waves propagating in the connecting microwave components and to reflection effects, which result from a certain mismatch in the relatively narrow bandwidths of the two JPCs. We also measure, at this working point, the maximum input power above which the device starts to saturate. We find it to be around -92 dBm which is comparable to the measured values in microstrip JPCs operated in frequency conversion [19].

Furthermore, in Fig. 3, we display a phase shift measurement of the transmitted signals through the device

in opposite directions, taken on resonance as a function of the applied phase difference φ . As seen from the data, the phase shifts of S_{21} and S_{12} vary in opposite directions and depend linearly on φ , which fully agree with the theoretical prediction. This result shows that the device not only can operate as a gyrator, but it can also serve as a general-purpose, nonreciprocal phase shifter, which can be fully and rapidly controlled *in situ* by a microwave signal, i.e., the pump.

In conclusion, we have implemented and measured a proof-of-principle, nonreciprocal phase shifter that does not employ any magnetic materials or strong magnets. The device is realized by coupling two dissipationless, nondegenerate Josephson mixers. By operating the Josephson mixers in frequency conversion mode, we show that the phase shift acquired by signals transmitted through the device can be controlled *in situ* by the phase difference of the pump drives feeding the two mixers. We also show that by setting the phase difference of the pump drives to $\pi/2$, the device can operate as a microwave gyrator. Both results are found to be in good agreement with the device theory.

Looking forward, the performance and size of such a nonreciprocal phase shifter can be significantly improved by eliminating the loss and delay between the two mixing stages. This can be achieved, for example, by integrating the two Josephson mixers on the same chip (or printed circuit board) in close proximity of each other and eliminating the need for bulky, off-chip, broadband hybrids, by using a hybrid-less version of these Josephson mixers [15]. Also, it is feasible to significantly enhance the instantaneous bandwidth of the device to more than 600 MHz, by utilizing impedance engineering techniques [22]. Such a lossless, nonreciprocal phase shifter and gyrator, which does not employ any magnetic materials or strong magnets for its operation, can be used in a variety of quantum information processing applications, ranging from *in situ* manipulation of microwave signals in superconducting circuits to the realization of on-chip circulators for routing signals in a quantum processor.

Acknowledgments

B.A. thanks Michel Devoret, Archana Kamal, and Michael Hatridge for discussions, and Christian Baks for the design and supply of PCBs used in mounting the JPC devices.

-
- [1] D. M. Pozar, *Microwave Engineering*, 3rd edition, (Wiley, Hoboken, NJ, 2005).
 - [2] A. Kamal, J. Clarke, and M. Devoret, *Nat. Phys.* **7**, 311 (2011).
 - [3] K. Sliwa, M. Hatridge, A. Narla, S. Shankar, L. Frunzio, R. Schoelkopf, and M. Devoret, *Phys. Rev. X* **5**, 041020 (2015).
 - [4] J. Kerckhoff, K. Lalumière, B. J. Chapman, A. Blais, and K.W. Lehnert, *Phys. Rev. Applied* **4**, 034002 (2015).
 - [5] Ranzani and J. Aumentado, *New J. of Phys.* **17**, 023024 (2015).
 - [6] F. Lecocq, L. Ranzani, G. A. Peterson, K. Cicak, R. W. Simmonds, J. D. Teufel and J. Aumentado, *arXiv:1612.01438*.

- [7] G. Viola and D. P. DiVincenzo, *Phys. Rev. X* **4**, 021019 (2014).
- [8] S. Bosco, F. Haupt, D. P. DiVincenzo, arXiv:1609.06543.
- [9] B. Abdo, K. Sliwa, L. Frunzio, and M. H. Devoret, *Phys. Rev. X* **3**, 031001 (2013).
- [10] B. Abdo, K. Sliwa, S. Shankar, M. Hatridge, L. Frunzio, R. Schoelkopf, and M. Devoret, *Phys. Rev. Lett.* **112**, 167701 (2014).
- [11] C. Macklin, K. O’Brien, D. Hover, M. E. Schwartz, V. Bolkhovskiy, X. Zhang, W. D. Oliver, and I. Siddiqi, *Science* **350**, 307 (2015).
- [12] M. R. Vissers, R. P. Erickson, H.-S. Ku, Leila Vale, Xian Wu, G. C. Hilton, and D. P. Pappas, *Appl. Phys. Lett.* **108**, 012601 (2016).
- [13] M. R. Vissers, R. P. Erickson, H.-S. Ku, Leila Vale, Xian Wu, G. C. Hilton, and D. P. Pappas, *Appl. Phys. Lett.* **108**, 012601 (2016).
- [14] <http://pamtechinc.com>
- [15] B. Abdo, J. M. Chavez-Garcia, M. Brink, G. Keefe, and J. M. Chow, arXiv:1609.00401.
- [16] B. Abdo, A. Kamal, M. H. Devoret, *Phys. Rev. B* **87**, 014508 (2013).
- [17] U. Vool, I. Pop, K. Sliwa, B. Abdo, C. Wang, T. Brecht, Y. Y. Gao, S. Shankar, M. Hatridge, G. Catelani, M. Mirrahimi, L. Frunzio, R. Schoelkopf, L. Glazman, and M. Devoret, *Phys. Rev. Lett.* **113**, 247001 (2014).
- [18] N. Ofek, A. Petrenko, R. Heeres, P. Reinhold, Z. Leghtas, B. Vlastakis, Y. Liu, L. Frunzio, S. Girvin, L. Jiang, M. Mirrahimi, M. Devoret, R. Schoelkopf, doi:10.1038/nature18949.
- [19] B. Abdo, K. Sliwa, F. Schackert, N. Bergeal, M. Hatridge, L. Frunzio, A. D. Stone, and M. Devoret, *Phys. Rev. Lett.* **110**, 173902 (2013).
- [20] E. Flurin, N. Roch, J. D. Pillet, F. Mallet, and B. Huard, *Phys. Rev. Lett.* **114**, 090503 (2015).
- [21] N. Roch, E. Flurin, F. Nguyen, P. Morn, P. Campagne-Ibarcq, M. Devoret and B. Huard, *Phys. Rev. Lett.* **108**, 147701 (2012).
- [22] T. Roy, S. Kundu, M. Chand, A. Vadiraj, A. Ranadive, N. Nehra, M. Patankar, J. Aumentado, A. Clerk, and R. Vijay, *Appl. Phys. Lett.* **107**, 262601 (2015).